ORGANIC LETTERS

2011
Vol. 13, No. 20
5632–5635

A Redox-Gated Slow-Fast-Stop Molecular Rotor

Cheng-Hua Yang, Ch. Prabhakar, Shou-Ling Huang, Ying-Chih Lin, Wei Shyang Tan, Nimesh C. Misra, Wei-Ting Sun, and Jye-Shane Yang*

Department of Chemistry, National Taiwan University, Taipei, Taiwan, 10617

jsyang@ntu.edu.tw

Received August 31, 2011

ABSTRACT

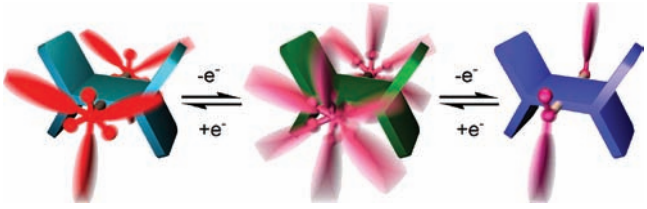

A pentiptycene-derived *p*-phenylenediamine mimics a molecular double-rotor system that displays redox-dependent rotation rates for the amino rotors about the pentiptycene-amine C−N bond. The rotation is accelerated in the radical cation state but stopped in the di(radical cation) state. Electronic interplay of the two rotors is also discussed.

p-Phenylenediamines (PPD) are a class of redox-active materials that undergo two-step oxidations to form the corresponding radical cation and dication species (Scheme 1). The unusual stability of PPD radical cations (e.g., Wurster's Blue) has attracted much attention, and their intriguing electronic properties such as magnetic susceptibility,[1] high-spin activity,[2] electron and energy transfer behavior,[3] fluorescence,[4] and electrostatic interactions[5] have been reported. Nevertheless, the potential application of PPD in forming redox-gated molecular devices[6] has not yet been demonstrated.

Scheme 1. Structure of *N,N,N′N′*-Tetramethyl-*p*-phenylenediamine and Its First (i.e., Wurster's Blue) and Second Oxidation States

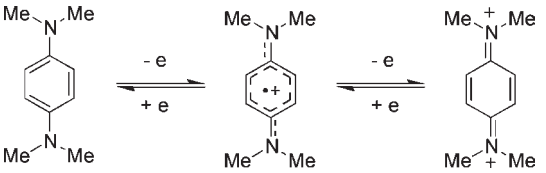

We have recently shown that the H-shaped pentiptycene scaffold[7] is useful for constructing light and electric powered molecular devices.[8] This stems from the presence of a central phenylene ring that can be derivatized to form a photochemically and/or electrochemically responsive π-conjugated unit. One important merit of these systems as

(1) Yamauchi, J.; Fujitha, H. *Bull. Chem. Soc. Jpn.* **1990**, *63*, 2928–2932.

(2) (a) Ito, A.; Taniguchi, A.; Yamabe, T.; Tanaka, K. *Org. Lett.* **1999**, *1*, 741–743. (b) Galecka, M.; Wielgus, I.; Zagorska, M.; Pawlowski, M.; Kulszewicz-Bajer, I. *Macromolecules* **2007**, *40*, 4924–4932. (c) Sakamaki, D.; Ito, A.; Furukawa, K.; Kato, T.; Tanaka, K. *Chem. Commun.* **2009**, 4524–4526.

(3) (a) Kaufman, F. B. *J. Am. Chem. Soc.* **1976**, *98*, 5339–5344. (b) Fernandez, E.; Blancafort, L.; Olivucci, M.; Robb, M. A. *J. Am. Chem. Soc.* **2000**, *122*, 7528–7533. (c) Grampp, G.; Justinek, M.; Landgraf, S.; Angulo, G.; Lukzen, N. *Photochem. Photobiol. Sci.* **2009**, *8*, 1595–1602. (d) Ito, A.; Sakamaki, D.; Ichikawa, Y.; Tanaka, K. *Chem. Mater.* **2011**, *23*, 841–850. (e) Tsuchiya, T.; Wielopolski, M.; Sakuma, N.; Mizorogi, N.; Akasaka, T.; Kato, T.; Guldi, D. M.; Nagase, S. *J. Am. Chem. Soc.* **2011**, *133*, 13280–13283.

(4) Grilj, J.; Laricheva, E. N.; Olivucci, M.; Vauthey, E. *Angew. Chem., Int. Ed.* **2011**, *50*, 4496–4498.

(5) Backer, M. D.; Hureau, M.; Depriester, M.; Deletoille, A.; Sargent, A. L.; Forshee, P. B.; Sibert, J. W. *J. Electroanal. Chem.* **2008**, *612*, 97–104.

(6) (a) Kottas, G. S.; Clarke, L. I.; Horinek, D.; Michl, J. *Chem. Rev.* **2005**, *105*, 1281–1376. (b) Kay, E. R.; Leigh, D. A.; Zerbetto, F. *Angew. Chem., Int. Ed.* **2007**, *46*, 72–191.

(7) Yang, J.-S.; Yan, J.-L. *Chem. Commun.* **2008**, 1501–1512.

(8) (a) Yang, J.-S.; Huang, Y.-T.; Ho, J.-H.; Sun, W.-T.; Huang, H.-H.; Lin, Y.-C.; Huang, S.-J.; Huang, S.-L.; Lu, H.-F.; Chao, I. *Org. Lett.* **2008**, *10*, 2279–2282. (b) Sun, W.-T.; Huang, Y.-T.; Huang, G.-J.; Lu, H.-F.; Chao, I.; Huang, S.-L.; Huang, S.-J.; Lin, Y.-C.; Ho, J.-H.; Yang, J.-S. *Chem.—Eur. J.* **2010**, *16*, 11594–11604. (c) Chen, Y.-C.; Sun, W.-T.; Lu, H.-F.; Chao, I.; Huang, G.-J.; Lin, Y.-C.; Huang, S.-J.; Huang, H.-H.; Lin, Y.-D.; Yang, J.-S. *Chem.—Eur. J.* **2011**, *17*, 1193–1200.

10.1021/ol202356t
Published on Web 09/30/2011

Scheme 2. Synthesis of **1** and **2**[a]

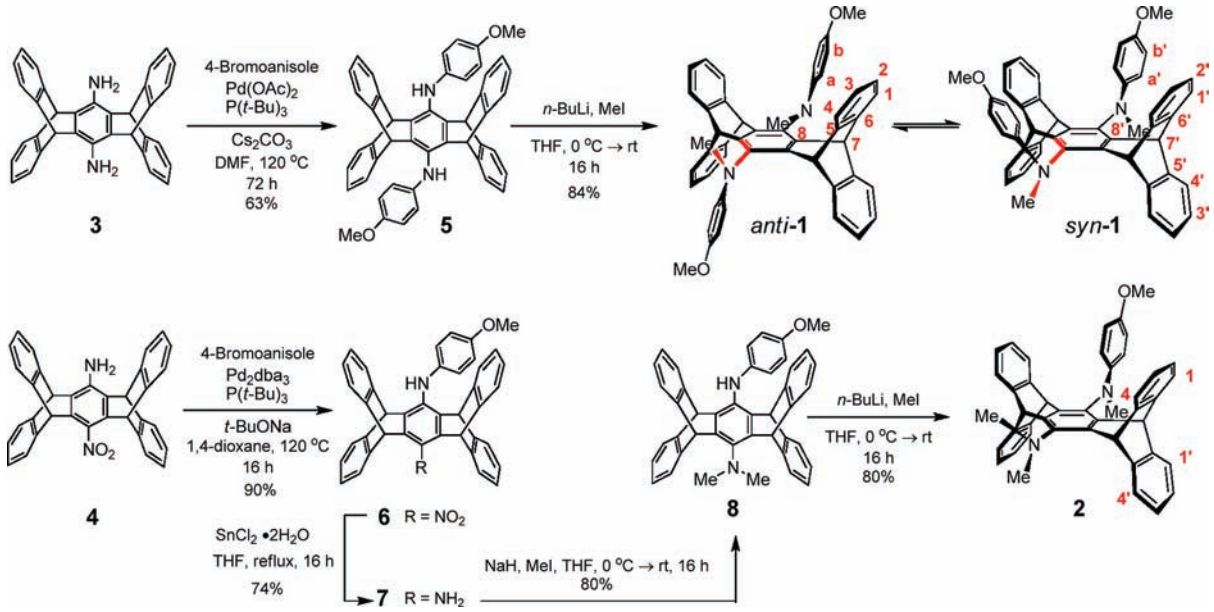

[a] The numberical labels for protons and carbons are for discussion of the VT NMR spectra. The C−C and C−N bonds in red color denote the C−C−N−C dihedral angles (α) discussed in the text.

compared to chemicals-fueled molecular devices is the absence of accumulation of chemical waste during the operation.[9]

We report herein a redox-controlled molecular double-rotor system (**1**) on the basis of the features of both pentiptycene and PPD. The interplay between the two rotors is evidenced by comparing **1** with the analog **2**. Both cyclic voltammetry (CV) and spectroelectrochemistry show that the second oxidation state of **1** retains the radical cation character, attributable to the bulky pentiptycene group that reduces the quinoidal character. DFT calculations suggested a dramatic change in rotation rates upon oxidation, and it is an acceleration for the first oxidation step but a brake function for the second oxidation process.

Compounds **1** and **2** were prepared by Pd-catalyzed *N*-arylation[10] of pentiptycenediamine **3** and **4**, respectively, with 4-bromoanisole followed by nitro group reduction and/or base-promoted *N*-methylation of the resulting products **5** and **6** (Scheme 2). The synthesis of both **3** and **4** has recently been reported.[11] The nitro group reduction in **6** → **7** was carried out with $SnCl_2$ in the presence of a catalytic amount of HCl. For the *N*-methylation reaction of **5** → **1**, *n*-BuLi is more favorable than weaker bases such as K_2CO_3 and NaH. However, an attempt to convert **7** directly to **2** with *n*-BuLi resulted in a mixture of unidentified compounds. Consequently, the triple *N*-methylation of **7** was accomplished by two reaction steps of first using NaH to form the intermediate **8** and then *n*-BuLi to introduce the third methyl group.

Two distinct conformations in the orientation of the two amino rotors are expected for **1**, and they are designated as *syn*-**1** and *anti*-**1** (Scheme 2). The presence of two *N*-Me signals of similar peak intensity (45:55) for the ^{1}H NMR spectrum of **1** in DMF-d_7 at ambient temperature suggests a slow interconversion and a similar energy of the two conformers. Indeed, DFT calculations[12] at the BMK/6-311+G(d,p)//B3LYP/6-31G(d) level suggested a small energy difference of 1.10 kcal mol^{-1} between *syn*-**1** and *anti*-**1** (Figure S1). The large calculated C−C−N−C dihedral angles (α = 86°, Table 1) defined by the central

Table 1. Structural Parameters of the Rotating Amino Rotor in DFT-Derived Ground State and Transition State of **1**, $\mathbf{1}^{+\bullet}$, and $\mathbf{1}^{2+}$

compd	state[a]	d_{C-N}[b]	θ_1[c]	θ_2[c]	θ_3[c]	θ_{sum}[c]	α[d]
1	GS	1.433	116.0	120.2	119.5	355.7	86.3
	TS	1.414	120.6	122.4	109.4	352.4	17.3
$\mathbf{1}^{+\bullet}$	GS	1.420	117.7	121.8	120.1	359.6	64.0
	TS	1.376	123.3	124.2	110.6	358.1	−8.0
$\mathbf{1}^{2+}$	GS	1.449	116.2	121.8	122.0	360.0	78.8
	TS	1.369	123.1	125.9	110.4	359.4	−13.1

[a] GS = ground state; TS = transition state. [b] C−N bond length in Å. [c] C−N−C bond angle in deg; θ_1 = C−N−C_{Me}; θ_2 = C−N−C_{Ph}; θ_3 = C_{Me}−N−C_{Ph}; θ_{sum} = $\theta_1 + \theta_2 + \theta_3$. [d] C−C−N−$C_{Me}$ dihedral angle in deg (see Scheme 2 for the red C−C and C−N bonds).

(9) (a) Raymo, F. M. *Angew. Chem., Int. Ed.* **2006**, *45*, 5249–5251. (b) Credi, A. *Aust. J. Chem.* **2006**, *59*, 157–169. (c) Saha, S.; Stoddart, J. F. *Chem. Soc. Rev.* **2007**, *36*, 77–92.

(10) (a) Wolfe, J. P.; Wagaw, S.; Marcoux, J.-F.; Buchwald, S. L. *Acc. Chem. Res.* **1998**, *31*, 805–818. (b) Hartwig, J. F. *Angew. Chem., Int. Ed.* **1998**, *37*, 2046–2067.

(11) Kundu, S. K.; Tan, W. S.; Yan, J.-L.; Yang, J.-S. *J. Org. Chem.* **2010**, *75*, 4640–4643.

(12) Frisch, M. J.; et al. *Gaussian 09*, Revision A.02; Gaussian, Inc.: Wallingford, CT, 2009.

phenylene C–C bond and the methyl N–C bond (Scheme 2) reveal significant steric congestion between the rotors and the stator in **1**.

The redox behavior of **1** was examined by CV, differential pulse voltammetry (DPV), spectroelectrochemistry, and chemical oxidation. Figure 1a shows the CV and DPV

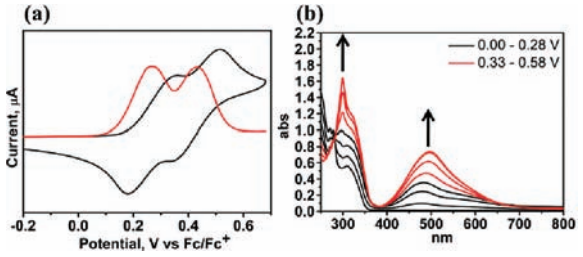

Figure 1. (a) Cyclic voltammogram (black) and differential pulse voltammogram (red) for oxidation of **1** in CH_2Cl_2 with electrolyte 0.1 M Bu_4NPF_6 at a scan rate of 100 mV s^{-1}, and (b) spectroelectrochemistry of **1** in acetonitrile at the first stage (black, 0.00, 0.18, 0.23, and 0.28 V vs Fc/Fc^+) showing an isosbestic point at 278 nm and at the second stage (red, 0.33, 0.38, 0.48, and 0.58 V vs Fc/Fc^+) showing an isosbestic point at 380 nm.

of **1** in dichloromethane (1 mM) containing 0.1 M Bu_4NPF_6. The voltammograms show two reversible redox processes (E_{ox} = 0.27 and 0.42 V vs ferrocene/ferrocenium redox couple) of the same current density, and the CV profile remains unchanged under multiple scans. Thus, the redox waves could be attributed to two single-electron transfer processes that form stable radical cation $\mathbf{1}^{+\bullet}$ and dication $\mathbf{1}^{2+}$. The difference in the two oxidation potentials (ΔE = 0.15 V) is much smaller than that of Wurster's Blue (ΔE = 0.59 V)[3a,5] or *N*,*N*′-diphenyl-*p*-phenylenediamine (ΔE = 0.53 V),[13] indicating weak interactions between redox sites. This is consistent with the twisted PPD moiety in **1** predicted by DFT calculations (Figure S1). Consequently, the second oxidation state of $\mathbf{1}^{2+}$ might be better described as a di(radical cation) species rather than the quinoidal form illustrated in Scheme 1. Figure 1b shows the absorption spectra of **1** under stepwise electrochemical oxidation. The new absorption band in 400–700 nm is characteristic of radical cations of PPD.[2,4,5] However, unlike the blue shifts of absorption sepctra commonly displayed by PPD on going from radical cations to dications,[5,13] it is red-shifted from 476 to 497 nm on going from $\mathbf{1}^{+\bullet}$ to $\mathbf{1}^{2+}$. This again reflects the di(raidcal cation) character of $\mathbf{1}^{2+}$. The two observed electrochemical oxidation states and their absorption spectra can also be generated by chemical oxidation[14] of **1** in acetonitrile with 1 and 2 equiv of $Cu(ClO_4)_2$, respectively (Figure S2).

Variable-temperature (VT) NMR studies and line-shape analysis on **1** were carried out to obtain activation parameters for the rotation of the NArMe rotors. DMF-d_7 was chosen as the solvent for measurements covering the temperature range of 243–363 K. The details of NMR peak assignments are supplied as Supporting Information (Figures S3–S9). In principle, the interconversion of *syn*-**1** and *anti*-**1** could be probed by nuclei in the amino rotors or in the peripheral phenylene rings of the stator (see Scheme 2 for nuclei labels). However, this is true only for the rotor nuclei (e.g., *N*-Me or C_a), because the syn–anti interconversion involves exchange of more than two nuclei in the stator (e.g., H_1 in *anti*-**1** is converted simultaneously to H_1 and H_4 in *syn*-**1**) and thus prevents a direct line-shape analysis. Therefore, only the syn–anti exchange rate (k_{ex}) is available for **1**. It should be noted that the k_{ex} value deduced from the rotor nuclei is not equivalent to the rotation rate (k_{rot}) of the rotors about the C–N bond. This is simply due to the fact that the reference point for considering k_{ex} and k_{rot} is different. The reference point is one of the two rotors in k_{ex}, but it is the pentiptycene stator in k_{rot}. In the extreme case of concerted rotations of both rotors at all times, the syn–anti exchange should not occur (i.e., $k_{ex} = 0$ albeit $k_{rot} \neq 0$). In the other extreme case of completely unconcerted rotations for the two rotors, it would be $k_{ex} = 2k_{rot}$. Since the real situation is more likely lying between the two extremes (i.e., $0 < k_{ex} < 2\,k_{rot}$), the $k_{ex}/2$ value should be considered as the lower limit of k_{rot} for the NArMe rotor in **1**. Figure 2 shows the experimental

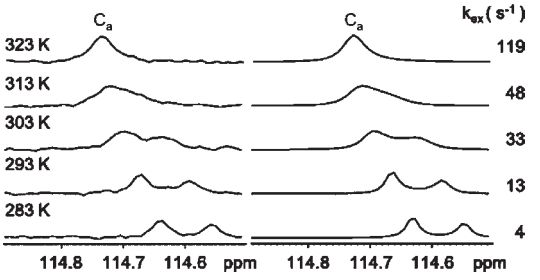

Figure 2. Experimental (left) and simulated (right) carbon VT NMR (125 MHz) spectra of the C_a signal of **1** in DMF-d_7. Values of temperature (T, K) and syn–anti exchange rate (k_{ex}, s^{-1}) are given for each trace.

and simulated VT ^{13}C NMR spectra of the C_a region, and the corresponding activation parameters retrieved from Arrhenius and Eyring plots (Figures S10 and S11) are shown in Table 2. Similar activation parameters are obtained on the basis of the *N*-Me proton signals (Figures S12 and S13). The small k_{ex} values (e.g., 48–50 s^{-1} at 313 K) and the high free energy of activation at 298 K ($\Delta G^{\ddagger}_{(298\ K)}$ = 15.7 kcal mol^{-1}) reflect a high degree of steric congestion in **1**.

Fortunately, the VT NMR spectra of **2** allow one to retrieve the k_{rot} of the NArMe rotor as well as the k_{ex} of the two rotors. The former was deduced from the line-shape analysis of the pentiptycene C_1–$C_{1'}$ and C_4–$C_{4'}$ signals, and the latter was from that of the two *N*-Me proton

(13) Nishiumi, T.; Nomure, Y.; Chimoto, Y.; Higuchi, M.; Yamamoto, Y. *J. Phys. Chem. B* **2004**, *108*, 7992–8000.
(14) Sumalekshmy, S.; Gopidas, K. R. *Chem. Phys. Lett.* **2005**, *413*, 294–299.

Table 2. VT ^{1}H an ^{13}C NMR Data and Activation Parameters for the Double-Rotor Systems **1** and **2**[a]

compound	**1**		**2**	
nucleus[b]	$H_{(N\text{-Me})}$[d]	C_a[d]	$H_{(N\text{-MeMe})}$[e]	$C_{(1,1';\ 4,4')}$[f]
T_c[c] (K)	313	313	253	353
$\Delta G^{\ddagger}_c$ (kcal mol^{-1})	15.9	15.9	12.9	16.9
E_a (kcal mol^{-1})	15.9 ± 1.1	14.4 ± 1.0	6.6 ± 0.3	13.6 ± 0.2
log A	12.9 ± 0.8	11.8 ± 0.8	7.7 ± 0.3	10.2 ± 0.2
$\Delta H^{\ddagger}$ (kcal mol^{-1})	15.3 ± 1.1	13.8 ± 1.0	6.2 ± 0.3	12.9 ± 0.4
$\Delta S^{\ddagger}$ (cal mol^{-1} K^{-1})	−1.6 ± 3.6	−6.5 ± 3.5	−25.0 ± 1.2	−14.0 ± 1.4
$\Delta G^{\ddagger}_{(298\text{K})}$ (kcal mol^{-1})	15.7 ± 1.6	15.7 ± 1.5	13.6 ± 0.5	17.1 ± 0.6
$k_{(313\ \text{K})}$ (s^{-1})	50	48	1106	5

[a] Recorded in DMF-d_7 unless otherwise noted. [b] For line shape analysis. See Scheme 2 for the nuclei labels. [c] Coalescence temperature. [d] Temperature range 283−323 K, 5 data points. [e] Recorded in CD_2Cl_2. Temperature range 203−273 K, 8 data points. [f] Temperature range 313−353 K, 5 data points.

signals in the NMeMe rotor (Figures S14−S17). The corresponding activation parameters are shown in Table 2. Because of the distinct difference in the k_{ex} and k_{rot} values at the same temperature (e.g., 1106 vs 5 s^{-1} at 313 K), we might conclude that the determined k_{ex} essentially corresponds to the k_{rot} of the NMeMe rotor. A larger k_{rot} value for the smaller rotor (NMeMe vs NArMe) reflects in part the N-substituent steric effect.

An intriguing phenomenon is manifested by the activation data in Table 2. According to the k_{ex} value (50 s^{-1}) of **1** at 313 K, the k_{rot} value for the NArMe rotor should be 25 s^{-1} or larger (i.e., $k_{rot} > k_{ex}/2$, *vide supra*). However, the determined k_{rot} value (5 s^{-1}) for the same NArMe rotor in **2** at 313 K is at least 5-fold lower. Evidently, the rotation rate of one rotor is strongly affected by the other rotor in PPD-based double-rotor systems. This is interesting but not unexpected, because the nature of the *N*-substituents could affect the electron density in the PPD moiety and thus the bond order and bond length of the C−N bond, which in turn affects the rotation barriers of the amino rotors.

The unusually large entropy effect (i.e., low log A and large negative $\Delta S^{\ddagger}$ values) observed for the NMeMe rotation in **2** also deserves attention. It appears that the transition state for the rotation is lowered by constraining the NArMe rotor. This again shows that electronic coupling between the two amino rotors plays an important role in determining the rotation kinetics.

Because of the paramagnetic character of both $\mathbf{1}^{+\bullet}$ and $\mathbf{1}^{2+}$,[15] the rotation kinetics of these oxidation states could not be evaluated by VT NMR. Accordingly, the structures and energies of the ground state (GS) and the transition state (TS) of **1**, $\mathbf{1}^{+\bullet}$, and $\mathbf{1}^{2+}$ along the amine rotation coordinates were evaluated by DFT calculations.[12,16] Table 1 shows the calculated pentiptycene-amino C−N bond length (d_{C-N}), bond angles about the N-atoms (θ_1−θ_3) and their sum (θ_{sum}), and C−C−N-C dihedral angles (α) of these states in the anti form. The DFT-predicted $\Delta G^{\ddagger}_{(298\ \text{K})}$ values for **1**, $\mathbf{1}^{+\bullet}$, and $\mathbf{1}^{2+}$ are 19.2, 13.8, and 29.7 kcal mol^{-1}, respectively. This corresponds roughly to a relative rotation rate of $1{:}10^4{:}10^{-8}$ for $\mathbf{1}{:}\mathbf{1}^{+\bullet}{:}\mathbf{1}^{2+}$ at room temperature. Assuming a rotation rate on the order of 10^2 s^{-1} for **1**, it becomes 10^6 and 10^{-6} s^{-1} for $\mathbf{1}^{+\bullet}$ and $\mathbf{1}^{2+}$, respectively, leading to a molecular rotor of three distinct (slow, fast, and stop) rotary mechanical states. Such a redox-gated acceleration and brake function for molecular rotors is, to our knowledge, unprecedented.

The relative d_{C-N} appears to play a critical role in determining the rotation barrier of this double-rotor system, as the shorter is the C−N bond, and the larger is the expected steric repulsion between the rotors and the stator. The C−N bond length is $\mathbf{1}^{2+}$ (1.449 Å) > **1** (1.433 Å) > $\mathbf{1}^{+\bullet}$ (1.420 Å) in the GS, but the order becomes **1** (1.414 Å) > $\mathbf{1}^{+\bullet}$ (1.376 Å) > $\mathbf{1}^{2+}$ (1.369 Å) in the TS. This is consistent with the highest rotation barrier for $\mathbf{1}^{2+}$ among the three redox states due to the least sterically hindered GS but most sterically hindered TS. Along this line, the GS should be destabilized more than the TS on going from **1** to $\mathbf{1}^{+\bullet}$ in order to account for the reduced torsional barrier. However, the difference in d_{C-N} for **1** vs $\mathbf{1}^{+\bullet}$ is more in the TS (0.038 Å) than in the GS (0.013 Å). This might indicate the presence of other factors that stabilize the TS more than the GS of $\mathbf{1}^{+\bullet}$. One possible factor is the increase in electronic delocaliztion for the TS vs GS due to the increased planarity in the PPD moiety (α = −8.0° vs 64.0°).

In summary, the first example of a PPD-based redox-active molecular device (**1**) is reported. The redox processes modify the electronic interactions and thus the rotation kinetics of the two rotors, which is a new mechanism for operating a molecular device.

Acknowledgment. We thank the National Science Council of Taiwan, ROC, for financial support.

Supporting Information Available. Experimental methods, synthetic procedures, compound characterization data, NMR peak assignments, complete experimental and simulated VT NMR spectra, ref 12, and DFT calculated data and coordinates. This material is available free of charge via the Internet at http://pubs.acs.org.

(15) DFT calculations suggest a triplet ground state for $\mathbf{1}^{2+}$. The phenomenon of broad ^{1}H NMR peaks for both $\mathbf{1}^{+\bullet}$ and $\mathbf{1}^{2+}$ is also consistent with a paramagnetic character.

(16) The method is justified by a reasonable agreement between the experimental and DFT (BMK/6-311+G(d,p)//B3LYP/6-31G(d)) calculated $\Delta G^{\ddagger}_{(298\text{K})}$ for the rotation of the NArMe rotor (17.4 vs 19.7 kcal mol^{-1}) and the NMeMe rotor (13.6 vs 15.8 kcal mol^{-1}) in **2**.